

## Supporting Information

# Rate-limited electroless gold thin film growth: a real-time study

*Gyoung Gug Jang, Phillip Blake and Donald Keith Roper\**

Ralph E. Martin Department of Chemical Engineering, 3202 Bell Engineering Center, University of Arkansas, AR 72701

\*To whom correspondence should be addressed. [Tel: +1 479 575 6691](tel:+14795756691). Fax: +1 479 575 7926.

E-mail: [dkroper@uark.edu](mailto:dkroper@uark.edu); [kroper@nsf.gov](mailto:kroper@nsf.gov)

### Table of Contents

- 1. Procedure to develop correlations between coefficients of mass transfer model and optical kinetic features as a function of Reynolds number.**
- 2. Quantitative XPS analysis of EL deposited films.**
- 3. Comparison between CF-EL and BI-EL plating.**
- 4. Thickness measurement of EL deposited films via SEM image analysis.**
- 5. Hydraulic effects on initiation of EL Au deposition.**
- 6. Correlation of dynamic transmission profile between 50 sec and 300 sec with mass transfer model.**
- 7. References.**

## 1. Procedure to develop correlations between coefficients of mass transfer model and optical kinetic features as a function of Reynolds number

1.1. Correlation between mass transfer coefficient (cm/s) profile and slope (%/s) of Au PL profile

- 1) Calculate Reynolds number for each CF-EL deposition.

$$Re = \frac{Q \times d_H}{\nu \times A_c}$$

where,  $d_H = 2h*w/(h+w)$ ,  $h$ =height of flow cell,  $w$ =width of flow cell,  $A_c$ = Cross section area of flow cell ( $w*h$ ),  $Q$  = volumetric flowrate ( $m^3/s$ ), and  $\nu$  = kinematic viscosity of Au solution.

The actual flow cell dimensions and their corresponding Reynolds numbers are summarized in Table S1.

- 2) Determine linear slopes of kinetic profiles of real-time Au PL transmission feature in the range of Au deposition using Excel. The Ag NP formation regime is excluded in the regression.
- 3) Develop a plot\_1 based on developed values of slopes versus Reynolds numbers
- 4) Calculate the deposition rate, mass transfer coefficient, of CF-EL deposition, using two different models( two compartment and rate model, equation (5) and film theory model, equation (6)), scalable flow cell dimensions, and related coefficients (Au(I) complex diffusivity and kinematic viscosity (assuming dilute Au solution)).
- 5) Plot the profile of mass transfer coefficients ( $k_i$  &  $k_m$ ) in the models as a function of Reynolds number with increasing injection flowrate. (Plot\_2)
- 6) Merge plot\_1 and plot\_2 with the result being Figure 4(B).

1.2. Correlation between specific deposited amount ( $M_{Au}/A$ ) profile and Au PL transmission drop profile

- 1) Calculate the Reynolds number for each CF-EL deposition.
- 2) Determine Au PL transmission drop value by quantifying *only* Au deposition regime (galvanic displacement & autocatalytic Au deposition). Exclude Ag NP formation regimes.
- 3) Develop a plot\_1 based on transmission drop values versus Reynolds numbers
- 4) Calculate the specific deposited amount ( $M_{Au}/A$ ) profile of CF-EL deposition, using two different models( two compartment and rate model, equation(5), thin film model, equation(6)), scalable flow cell dimensions, mass flux balance equation (equation(7)) and related coefficients (Au(I) complex diffusivity, viscosity).

- 5) Plot the profile of specific deposited amount in the models as a function of Reynolds number with increasing injection flowrate. (Plot\_2)
- 6) Merge plot\_1 and plot\_2 and result in Figure 4(A).

Table S1 is a summary of cell dimensions, deposition conditions, Reynolds numbers and optical observations from each CF-EL deposition. Figure S1 depicts optical transmission profile of each CF<sub>w</sub>-EL sample with slope descriptions.

**Table S1.** A summary of cell dimensions, deposition conditions, Reynolds numbers and optical observation form each CF-EL deposition.

	<b>CFw-2-10</b>	<b>CFw-3-10</b>	<b>CFw-4-10</b>	<b>CFw-5-10</b>	<b>CF-3-10</b>
Cell dimension (W×H×L, mm <sup>3</sup> ) (measured width)	<b>~2.7×1.0×31.2</b> (2.76/2.65/2.72/2.70)	<b>~2.3×1.0×31.8</b> (2.35/2.25/2.41/2.31)	<b>~2.8×1.0×31.5</b> (2.78/2.84/2.84/2.78)	<b>~2.3×1.0×31.2</b> (2.23/2.23/2.29/2.33)	<b>~1.7×1.0×32.0</b> (1.64/1.71/1.70/1.76)
Flowrate (Q, ml/hr)	<b>2</b>	<b>3</b>	<b>4</b>	<b>5</b>	<b>3</b>
Re (Qd <sub>H</sub> /vA <sub>c</sub> )	<b>~0.3</b> (0.29~0.31)	<b>~0.505</b> (0.49~0.52)	<b>~0.585</b> (0.57~0.60)	<b>~0.875</b> (0.85~0.90)	<b>~0.64</b> (0.62~0.66)
Slope(%/s) of transmission profile at 495nm (10~610s)	<b>-0.084 (R<sub>2</sub>=0.995)</b>	<b>-0.090 (R<sub>2</sub>=0.996)</b>	<b>-0.094 (R<sub>2</sub>=0.974)</b>	<b>-0.121 (R<sub>2</sub>=0.963)</b>	<b>-0.112 (R<sub>2</sub>=0.922)</b> (26~626s)*
Slope(%/s) of transmission profile at 495nm (50~300s)	<b>-0.089 (R<sub>2</sub>=0.991)</b>	<b>-0.099 (R<sub>2</sub>=0.999)</b>	<b>-0.127 (R<sub>2</sub>=0.990)</b>	<b>-0.160 (R<sub>2</sub>=0.997)</b>	<b>-0.143 (R<sub>2</sub>=0.995)</b> (70~300s)*
Drop(%) of transmission at 495nm (10~610s)	<b>45.9</b>	<b>53.0</b>	<b>59.3</b>	<b>69.7</b>	<b>64.9</b> (26~626s)*
Slope(%/s) of transmission profile at 425nm (10~610s)	<b>-0.098 (R<sub>2</sub>=0.992)</b>	<b>-0.107 (R<sub>2</sub>=0.996)</b>	<b>-0.120 (R<sub>2</sub>=0.966)</b>	<b>-0.147 (R<sub>2</sub>=0.956)</b>	<b>-0.120(R<sub>2</sub>=0.925)</b>
Drop(%) of transmission at 425nm (10~610s)	<b>51.0</b>	<b>56.8</b>	<b>64.2</b>	<b>76.2</b>	<b>60.5</b>

\*Teflon tape is compressible with the range of h= 0.8 ~1.0 mm, Kinematic viscosity(v) of diluted Au solution is assumed to be 0.01004 cm<sup>2</sup>/s

\* For CF-3-10, the estimated time regime of Au related deposition is between 26 and 626sec.

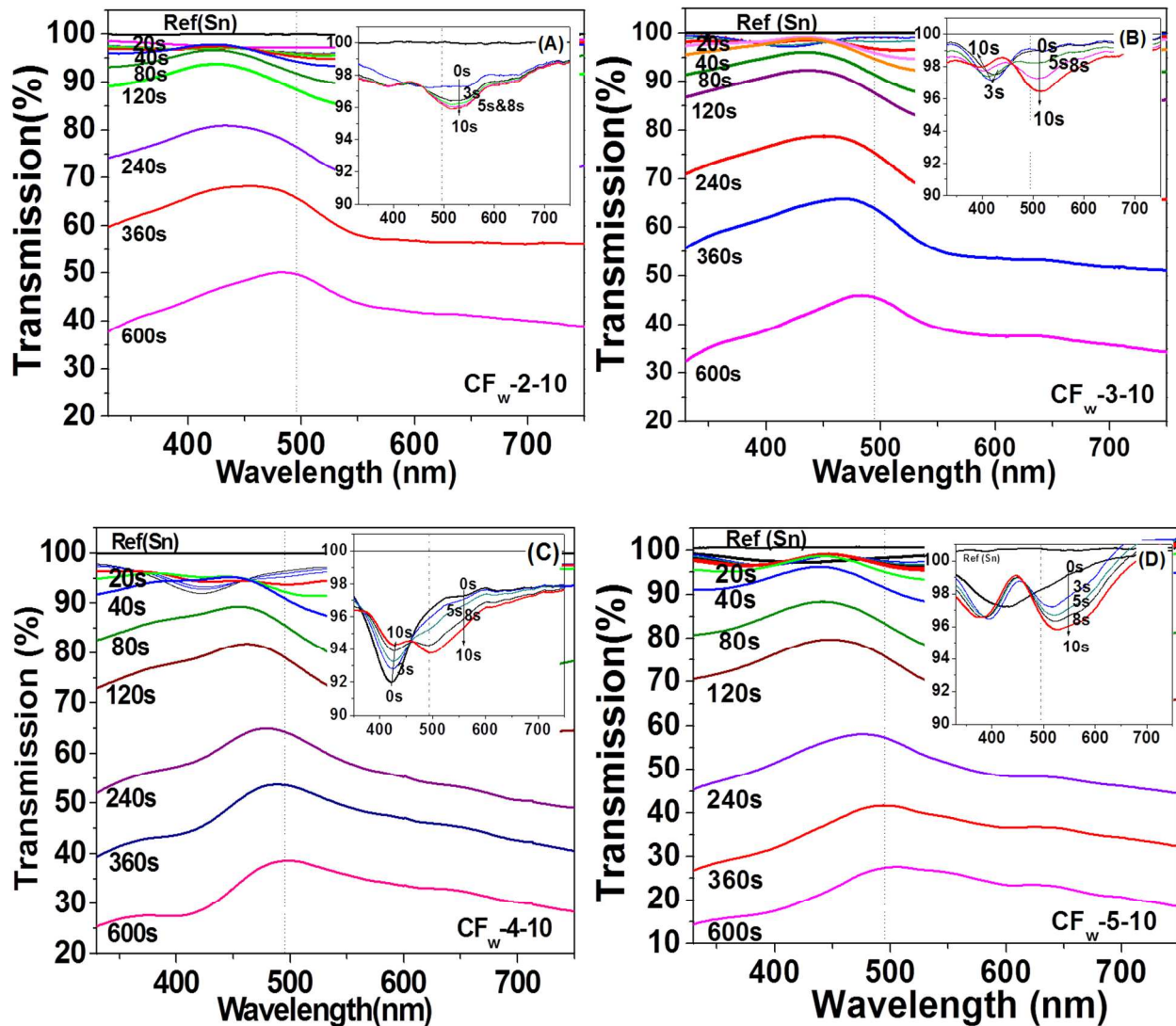


**Figure S1.** Time resolved transmission spectra during an entire plating of (A)  $CF_w$ -2-10, (B)  $CF_w$ -3-10, (C)  $CF_w$ -4-10 and (D)  $CF_w$ -5-10. Dotted lines indicate 495 nm position used for calculations. Inset is a close-up spectra between 0 s and 10 s.

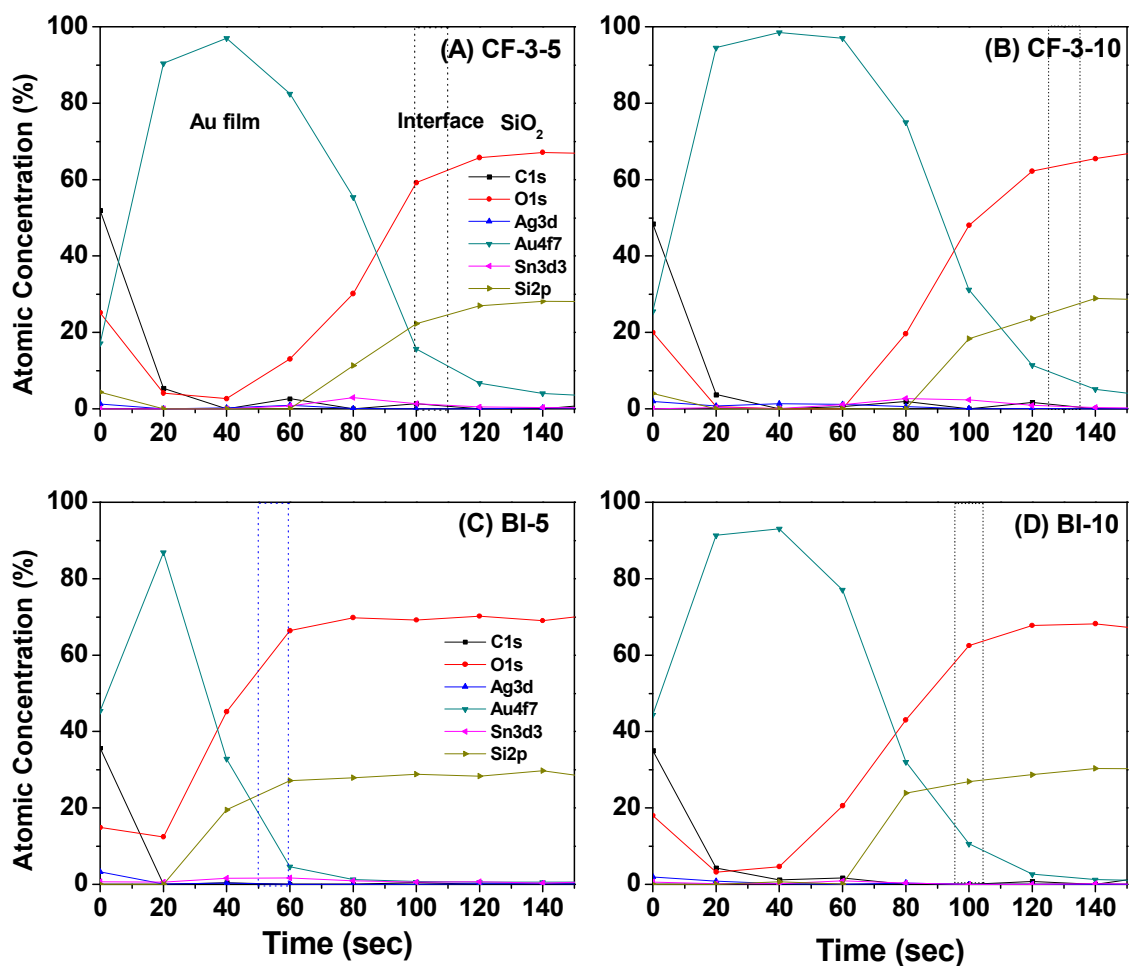
## 2. Quantitative XPS analysis of EL deposited films.

Figure S2 compares the quantitative atomic % composition of CF- and BI-EL films during intermittent 20 sec depth profiling for total 150 sec. For CF-3-5, shown in Figure S2(A), at the surface (0 sec sputtering), Au content is ~17.2 % due to organic carbonate contamination from adhesives and silver oxide particle residue, 52.0% of C, 25.1% of O, 1.3% of Ag and 4.4% of Si. After 20 sec sputtering, the Au concentration dramatically increased to 83.7 % as the sputtering had removed nearly all the organic contaminants (C and O content decreases to 9.9 and 4.1%, respectively). A continued increase in Au content to 89.7% is observed after 40 sec sputtering with C and O content further decreased to 5.5% and 3.5%. This composition represents the internal structure of the EL Au film. After 60 sec, Au content decreases to 81.5% due to an increase of oxygen content to 7.9%, which is believed to originate from metal oxides such as Au, Ag (0.8%) and Sn (3.4%). Sn content suddenly increased from 0.3% at 40 sec of sputtering to 3.4%. No Si was detected at this sputtering step. After 80 sec, Au content decreases to 44.7 %, while O, Si and Sn increase to 34.0%, 10.4% and 4.6%, respectively. After 100 sec, the content of O (59.5%) and Si (20.4%) exceed Au content (14.6%). Interestingly, the Sn content decreases to 2.5%. This observation suggests that the substrate-film interface of the CF-3-5 film is reached between 80~100 sec of Ar sputtering. The interface area is indicated by dot box in Figure S2(A). Between 120 and 240 seconds, the O, Si, and Na content stabilize at ~64.4 %, ~27.3 %, and ~2.3 %, representing the composition of the soda lime silica glass substrate.

Other EL films' atomic concentration profiles also exhibit similar patterns for distinguishable structural features such as surface, internal structure of Au film, interface and SiO<sub>2</sub> substrate. However, the interface locations or film thickness are dependent on different amounts of Au mass transferred induced by varying deposition time and hydrodynamic conditions. Using the

main components (Au, O and Si) % distributions, the location of interface composition was assigned to below 10% of Au and more than 30% and 15% of O and Si. Based on this standard the interface of BI-5, BI-10, CF-3-5 and CF-3-10 are assigned to ~55, ~100, ~100 and ~130 sec. The hydrodynamic comparison clearly shows that the thickness of CF-EL films is higher than BI-EL films at the same deposition time. The increased mass transfer rate and steady, higher average local concentration for CF increase the amount deposited relative to batch immersion, resulting in thicker films.

The values summarized in Table S1 and S2 are used to predict depth profiles in Figure 2. The predicted profiles of Figure 2(B) are developed based on BI-EL models (eqn (3)&(4)) and CF-EL models (eqn(5)&(6)&(7)).



**Figure S2.** Quantitative chemical component characterization of XPS depth profile of two different CF and BI deposited film for 5 and 10 min. Target chemical components are C1s, O1s, Ag3d, Au4f7, Sn3d3 and Si2P.

**Table S2.** Summary of BI-EL and CF-EL deposition and measured thickness (XPS & SEM)

	<b>BI-5</b>	<b>BI-10</b>	<b>CF-3-5</b>	<b>CF-3-10</b>
<b>Cell dimension (W×H×L, mm<sup>3</sup>)</b>	<b>~1.9×1.0×32.0</b>	<b>~1.8×1.0×32.0</b>	<b>~1.9×1.0×32.0</b>	<b>~1.7×1.0×32.0</b>
<b>Flowrate (Q, mL/hr) / deposit time (min)</b>	<b>0 ml/hr / 5 min</b>	<b>0 ml/hr / 10 min</b>	<b>3ml/hr / 5 min</b>	<b>3 ml/hr/ 10 min</b>
<b>Re (Qd<sub>fil</sub>/vA<sub>c</sub>)</b>	<b>--</b>	<b>--</b>	<b>~0.595 (0.58~0.61)</b>	<b>~0.64 (0.62~0.66)</b>
<b>Predicted thickness (M<sub>Aw</sub>/(A*ρ)), (nm)</b>	<b>27.1 / 27.4 (Semi-infinite / Finite slap)</b>	<b>35.6 / 38.8 (Semi-infinite/ Finite slap)</b>	<b>44.6 / 43.8 (Two-comp./ Film)</b>	<b>89.3 / 87.8 (Two-comp./ Film)</b>
<b>Sputtering time to substrate (s)</b>	<b>~55</b>	<b>~100</b>	<b>~100</b>	<b>~130</b>
<b>Measured thickness (nm) (XPS)</b>	<b>16.7 ~ 33.3</b>	<b>33.3 ~ 66.7</b>	<b>33.3 ~ 66.7</b>	<b>43.3 ~ 86.7</b>
<b>Measure thickness (nm) (SEM)</b>	<b>25.4±7.6</b>	<b>47.5±12.8</b>	<b>44.2±11.3</b>	<b>88.0±13.2</b>

### 3. Comparison between CF-EL and BI-EL plating.

Figure S3 shows kinetic profiles which consist of discrete measures of transmission at 425 nm (dotted lines) and 495 nm (solid lines), corresponding to the known Ag LSPR and Au PL features, taken in real time during EL Au deposition. Blue and red lines correspond to plating by batch immersion for 10 minutes (BI-10) and by continuous flow plating at 3 mL/min for 10 minutes (CF-3-10), respectively. Each temporally discrete measure of transmission was obtained from a real-time spectra from 330 to 750 nm obtained *in situ*. For both CF-3-10 and BI-10, Ag was deposited for 2 min onto Sn-sensitized silicate glass (during which spectra, not shown, were obtained at 30-sec intervals) and washed for 5 min with H<sub>2</sub>O before initiating EL Au deposition at time 0 sec. BI-10 plating was performed in the same system as CF-3-10 by displacing the entire system volume of 0.5 mL in 1 sec with Au plating solution, incubating for 10 min and successive H<sub>2</sub>O washing of entire volume with 0.5 mL for 10 sec. Each kinetic profile consists of the period of 30 sec H<sub>2</sub>O washing before Au solution injection, consecutive 600 sec Au deposition and subsequent H<sub>2</sub>O washing and incubation for 100 sec. Particularly, the observed longer profile of CF-3-10 than BI-10 is due to lateral diffusion of Au (I) ions and HCHO ions in continuous flow during a lag time. There was a volumetric holdup of ~72  $\mu$ L in the injection system between glass syringes containing Au solution and the spectroscopic flow cell. At 3 mL/hr flowrate, this resulted in a theoretical lag of ~87 seconds.

SEM images in Figure S3 show representative morphologies of CF-EL thin metal films corresponding to time regimes of EL deposition at -10 sec (I), 27 sec (II) and 670 sec (III), respectively, or in other words 10 sec before Au deposition began, 27 sec after Au deposition began, and 70 sec after Au deposition ended. Representative images I and II are 2 min Ag

activated films and HCHO driven Ag NPs which were produced in separate Ag activation and post HCHO exposure experiments with the same hydraulic conditions. Image III is a 10 min CF-EL Au deposited film. Figure S3 inset contains representative spectra for CF-3-10 at time points indicated by arrowheads on the profile in the main figure. The dot and solid lines in the inset indicate 425 nm (characteristic Ag LSPR feature point) and 495 nm (Au PL feature point) wavelengths, respectively. At time point I (-10 sec) in the CF-3-10 profile, transmission at 495 nm is ~90 %. This point corresponds to the inset transmission spectra at -10 and 0 sec (black) which exhibit a broad valley with a minimum at ~495 nm, attributable to deposition of thin metallic Ag island film which shows a broad absorption peak at ~500-520 nm.<sup>1,2</sup> At time point II, transmission at 495 nm is ~69%. This point corresponds to the inset transmission spectra at 27 sec (pink), attributable to transformation of Ag thin film to Ag NP via reduction resulting from 2.7× faster diffusive flux of methylene glycol (hydrated HCHO) to the Ag surface, relative to the diffusion of Au(I) sulfite complex.<sup>8</sup> Formaldehyde (HCHO), an electron donor for EL plating, reduces Au(I) to Au(0) and Ag(I) to Ag(0).<sup>3</sup> Active Ag ions remaining at the Ag island surface reduce Ag(0) and lead to self-assembled Ag NPs via concomitant reduction from Sn(IV) to Sn(II) at the interface between Ag and Sn(IV) wetted substrates.<sup>8</sup> The mass transfer rate calculated by equation (5) for these hydraulic conditions for methylene glycol ( $\sim 6.2 \times 10^{-4}$  cm/s) is 2-fold faster than Au(I) sulfite complex ( $\sim 3.2 \times 10^{-4}$  cm/s). At time point III (670 sec), transmission at 495 nm is ~5%. The corresponding transmission spectra exhibit a peak at ~495 nm (not shown), similar to the feature observed at 200 sec. Continuous Au films have a characteristic PL transmission peak near 500 nm.<sup>4,5</sup>

Analysis of characteristic profile features such as slope fluctuations allows the time-scales of discrete EL film growth regimes to be identified and quantified. Similar kinetic profile

trends, as shown in Figure S3, are observed during initial EL plating period (0-100 sec) for both CF-3-10 and BI-10. For CF-3-10, this period is characterized by a rapid decrease in transmission profiles at 495 nm (0-15 sec), followed by a steady decrease (16-36 sec), and finally another deep decrease of profiles (37-100sec). The transmission profile at 425 nm also shows three fluctuations such as a rapid drop (0-27 sec), a steady increase (28-84 sec), and a final decrease (85-100 sec). Similar fluctuation patterns are observed in the BI-10 transmission profile. The profile at 495 nm (blue) exhibits a rapid drop (0-5 sec), a steady decrease (6-20 sec) and another deep drop (21-100sec). For the profile at 425 nm, BI-10 also follows the trends of CF-3-10 which are characterized by drop, increase and another decrease during initial 100 sec deposition. Close-up profiles at 425 nm between 0 and 80 sec are shown in Figure S4. These three distinctive fluctuations are indicative of three successive EL Au film formation regimes: HCHO driven Ag NP formation, Ag-Au alloy formation via galvanic displacement of Ag by Au and autocatalytic Au film growth.

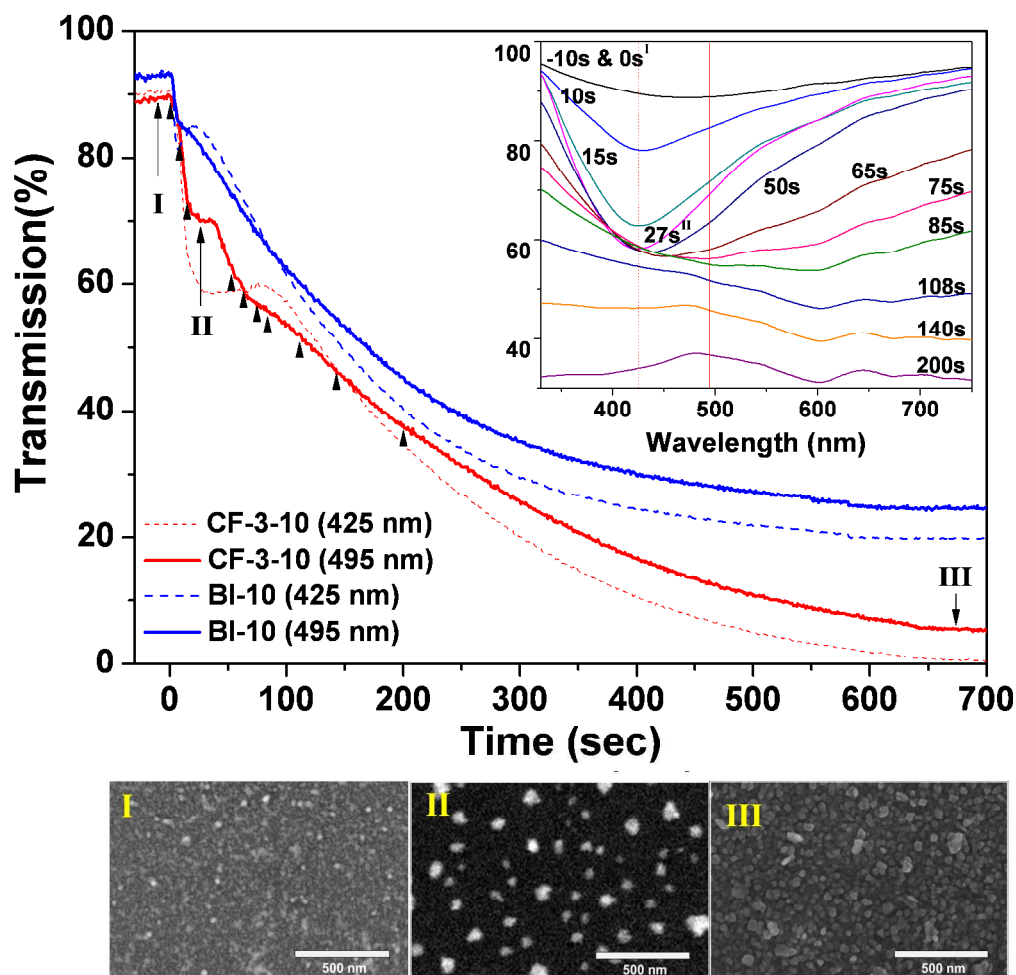
For CF-3-10, the kinetic transmission profiles at 425 nm and at 495 nm include Ag and Ag-Au alloy LSPR feature from 0 to 85 sec, and Au PL feature after 85 sec. The transmission profile at 425 nm decreases more rapidly than the transmission profile at 495 nm for 0 to 27 sec, the first regime, because of the appearance of an Ag LSPR absorption peak induced by Ag NP formation via HCHO reduction, as shown in Figure S3 SEM image II. Figure S3 inset shows the transmission spectra rapidly changed from an Ag film feature with a broad valley at circa 500 nm at 0 sec to an LSPR absorption feature of Ag NPs with a narrower, more intense valley depth at 425 nm at ~27 sec. During the second regime, between 28 sec and 85 sec, the transmission profile at 425 nm slowly increases and the transmission profile at 495 nm decreases with different slopes. The corresponding inset transmission spectra at 50 sec, 65 sec, and 75 sec

indicate a redshift in the Ag LSPR absorption valley to 507 nm with broadening. This redshift and broadening of the Ag plasmon features are attributed to Ag-Au alloy formation during galvanic displacement of Ag by Au.<sup>6,7</sup> Clear indications of galvanic displacement termination is accompanied by a simultaneous rise in the Au PL peak at ~480 nm, as shown in the inset transmission at 85 sec. After this point, the transmission profile at 495 nm is indicative of a characteristic Au PL feature. The third regime, autocatalytic Au film growth, began with a smooth transmission profile decrease. The Au PL feature became distinguishable at a wavelength of ~480 nm and the overall valley feature dramatically transformed to peak feature at 108 sec. From this time, growth of the Au island film structure eventually results in island coalescence which creates a continuous path for electrons throughout the Au network, resulting in significant changes in the optical and electrical film properties.<sup>7</sup> Further increases in deposition time resulted in a redshift of the Au PL peak to 495 nm with an increasing peak height, which is consistent with growth of an Au island film structure.<sup>8</sup> At 108 sec, a peak appeared at 650 nm which may be attributed to surface plasmon polaritons (SPPs) due to increased film thickness up to ~50 nm.

The kinetic profiles of BI-10 exhibit similar trends to those of CF-3-10, albeit within a shorter time period for the first (0-5 sec) and second (6-20 sec) regimes, suggesting the deposition mechanism is the same for both EL plating methods. The shorter time regime in BI-10 is due to instant solution injection prior to 10 min incubation. Instant injection induces a brief CF effect, which leads to a faster initial mass transfer rate of HCHO and Au complex ions than for constant injection flow in CF-3-10. This results in faster HCHO-driven Ag NP formation and successive galvanic displacement of Ag by Au. Detailed spectral information for these regimes for BI-10 is shown in Figure S4.

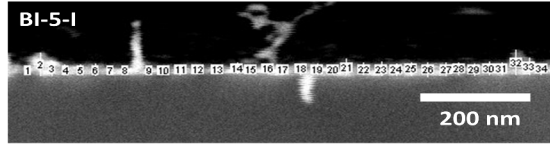
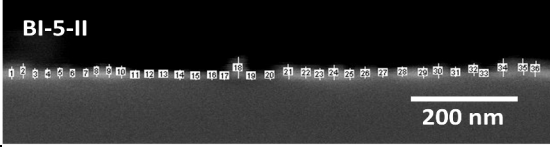
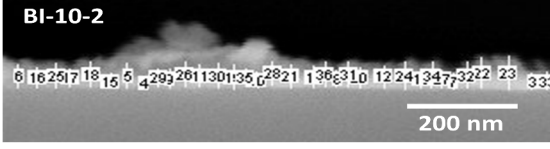
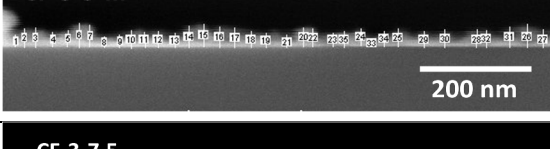
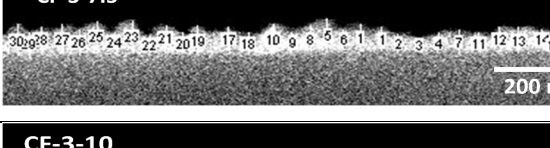
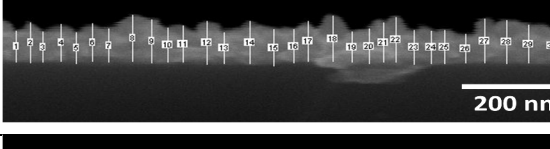
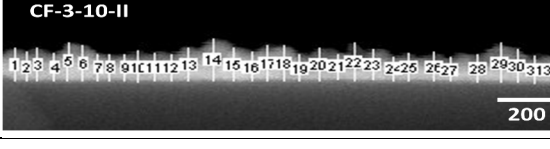
Overall kinetic profile of CF-EL exhibits steady state deposition. The overall kinetic Au plasmon transmission profile in Figure S3 supports that the mass transfer rate of CF-EL deposition is consistently higher than BI-EL. BI-EL Au mass transfer is a time dependent diffusion model, as explained above, because of species depletion over time. In principle, BI-EL deposition rate decreases exponentially as deposition time increases (see finite slab and semi-infinite BI profile in Figure 2(B)). The kinetic transmission profile at 425 nm and 495 nm of BI-10 clearly exhibit non-linear regressions corresponding with the BI mass transfer models. For the transmission profile at 425 nm, linear regression yields a decreasing slope of  $-0.105 \text{ \%}/\text{sec}$  ( $R^2 = 0.827$ ) between 6 and 606 sec. The first Ag LSPR feature regime (0~5 sec), specifically HCHO driven Ag NP formation region, was excluded from the regression. The second regime (6~20 sec), Ag-Au alloy regime via galvanic displacement, was included in the regression because of Au involvement. (not straight line) The slope between 6 and 606 sec in transmission profile at 495 nm was assigned to a Au PL feature profile which exhibits a similar value of  $-0.094$  ( $R^2 = 0.851$ ). However, the kinetic profile of CF-3-10 is different from that of BI-10. The mass transfer rate for CF-EL Au deposition is steadily higher than BI-EL deposition due to adjacent, continuous laminar flow for 600 sec. This flow decreases the stagnant boundary layer thickness adjacent to the wall and provides a time-invariant Au concentration. Theoretically, the total deposited amount of Au ions is linearly increasing during Au deposition due to constant deposition rate (see the red line and dot in Figure 2(B)). The kinetic profiles of CF-3-10 at 425 nm and 495 nm (Au PL) exhibit a more linear nature than BI-10 resulting in 425 nm transmission profile slope of  $-0.120$  ( $R^2=0.925$ ) and an Au PL profile slope of  $-0.112$  ( $R^2=0.922$ ) between 26 and 626 sec. Similar to the BI samples, the HCHO driven Ag formation (0~25 sec) was excluded from the regression while the Ag-Au alloy regime (26~85 sec) was included.

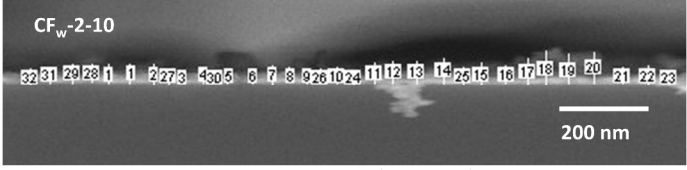
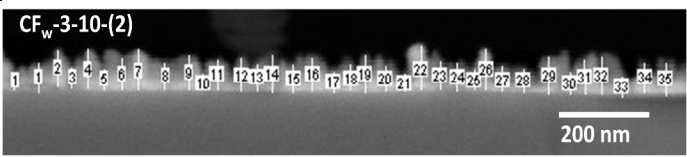
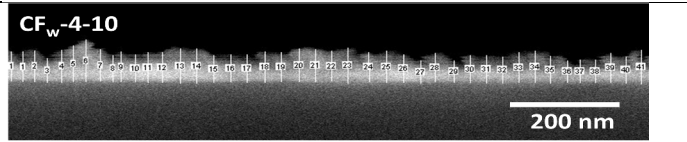
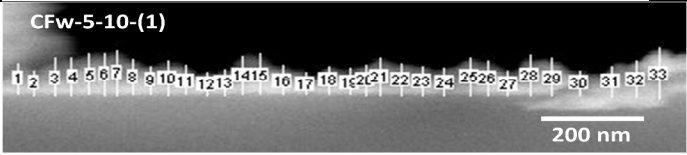
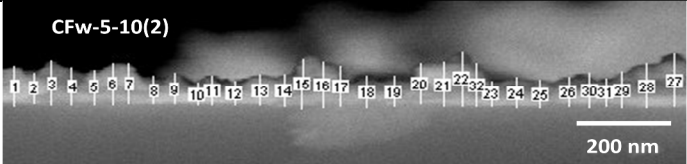
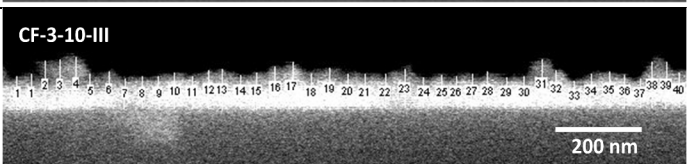
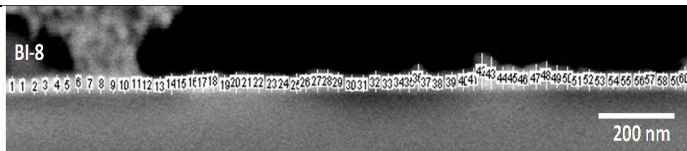
These more linear and steeper slopes for CF-3-10 profiles appear to correlate with the proposed mass transfer model for CF-EL systems.



**Figure S3.** Kinetic profiles of real-time Ag LSPR and Au PL transmission feature at 425 and 495 nm for CF and BI-EL Au deposition. Inset are transmission CF-EL spectra taken at times indicated by the black arrows in the main figure. Dotted and solid lines in the inset identify 425 nm and 495 nm wavelengths from which profiles in the main figure were derived. SEM images show representative EL metal film morphologies during three steps in EL Au plating: I. Ag cluster deposited film (-10 sec); II. HCHO-driven Ag NP formation (27 sec); III. EL Au deposited film (670 sec))

#### 4. Thickness measurement of EL deposited films via SEM image analysis.

Sample	Image	Sample Length	Foot size	Thickness
BI-5-I (339s)		~1μm	30 nm	28.9 ±8.2 (n=34)
BI-5-II (302s)		~1μm	30nm	25.4 ±7.6 (n=36)
BI-10-I (607s)		~1μm	30nm	47.5 ±12.8 (n=33)
BI-10-I (600s)		~1μm	30nm	53.0 ±11.8 (n=34)
CF-3-5-I (337s)		~1μm	30nm	44.2 ±11.3 (n=33)
CF-3-5-II (350s)		~1μm	30nm	42.7 ±8.6 (n=33)
CF-3-5-III (312s)		~1μm	30nm	38.0 ±9.6 (n=33)
CF-3-7.5-I (469s)		~1.3 μm	~40 nm	60.6 ±11.1 (n=33)
CF-3-10-I (625s)		~1.3 μm	~40 nm	88.0 ±13.2 (n=34)
CF-3-10-II (637s)		~1.3 μm	~40 nm	83.6 ±13.2 (n=33)

Sample	Image	Sample Length	Foot size	Thickness
CF <sub>w</sub> -2-10 (630s)		~1.3μm	35 nm	45.3 ±9.6 (n=34)
CF <sub>w</sub> -3-10(1) (630s)		~1.3μm	35nm	53.4 ±13.0 (n=33)
CF <sub>w</sub> -3-10(2) (630s)		~1.3μm	35nm	66.8 ±14.9 (n=34)
CF <sub>w</sub> -4-10 (600s)		~1.2μm	25nm	71.0 ±10.1 (n=42)
CF <sub>w</sub> -5-10(1) (600s)		~1.3μm	35nm	95.6 ±21.9 (n=33)
CF <sub>w</sub> -5-10(1) (600s)		~1.3μm	35nm	83.4 ±17.1 (n=33)
CF-3-10-III (632s)		~1.6 μm	30nm	90.5 ±15.3 (n=42)
BI-8 (490s)		~1.8μm	25nm	41.4 ±8.1 (n=62)

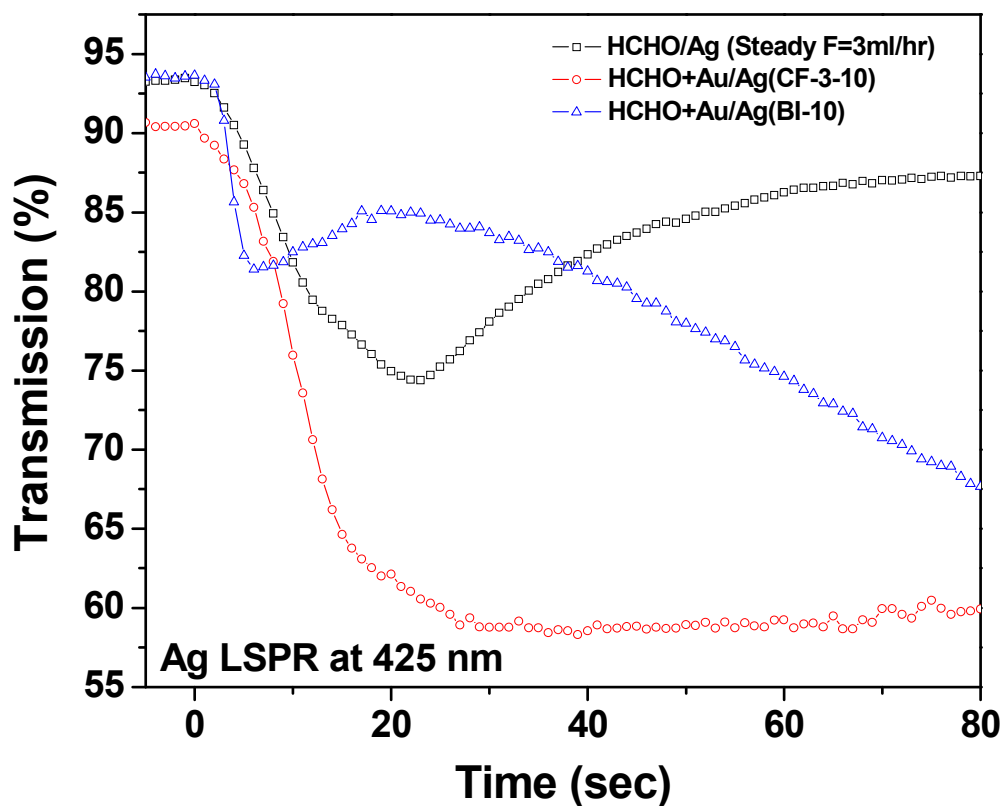
## 5. Hydraulic effects on initiation of EL Au deposition.

Hydraulic differences in the diffusion rate between CF and BI EL samples affect the rates of reaction throughout the plating process. The shorter initial fluctuation period of BI-10 relative to CF-3-10 may be due to less activated Ag amount, which can be inferred by higher transmission value at 0 sec in Figure 3 for BI-10, and faster mass transfer rate during the initial instantaneous Au solution injection in 1 sec. Figure S4 compares three different kinetic profiles of Ag LSPR transmission at 425 nm, CF-3-HCHO (square), CF-3-HCHO+Au (CF-3-10, circle) and BI-HCHO+Au (BI-10, triangle) to characterize hydraulic and chemical components effect during the early stages of EL deposition. For the CF-3-HCHO profile, HCHO treatment of a Ag activated substrate with a flow rate of 3 ml/hr for 5 min, shows three distinctive regimes which may be ascribed to Ag NP aggregation, Ag NP ripening and photosensitive Ag NPs erosion. The profile was captured between 0 and 80 sec for clarity. In complete dark treatment, the transmission reduced to 60 % after 5 min HCHO treatment.<sup>8</sup> Light sensitive Ag ions are photochemically reduced to metallic Ag clusters in the presence of trace halides with UV exposure.<sup>9</sup> UV exposure in wideband spectra light induces reduction of light sensitive Ag ion in bulk solution, which interferes with aggregation into larger particles on the surface. Therefore, the transmissivity of CF-3-HCHO recovered due to removal of aggregated larger Ag NPs via UV-exposure and concomitant washing flow and leaving behind smaller particles associated to the surface. The CF-3-HCHO+Au profile exhibits similar trends to CF-3-HCHO with analogous slopes during the first two regimes. For the CF-3-HCHO+Au system, the reductant, HCHO, may contact reduced Ag film in advance of Au(I) complex ion due to the lower mass transfer rate of the latter ion through a stagnant boundary layer of H<sub>2</sub>O. From calculated diluted HCHO and Au(I) complex diffusivity, the theoretical mass transfer rate of CH<sub>2</sub>(OH)<sub>2</sub>, a hydration form of HCHO

( $6.2 \times 10^{-4}$  cm/s), is  $\sim 2$  times higher than Au(I) complex ( $3.2 \times 10^{-4}$  cm/s) in the CF-3-HCHO+Au system. During the fast Ag aggregation regime via fast HCHO contact, the slope of CF-3-HCHO+Au (-1.24 %/sec) is similar to that of CF-3-HCHO deposition (-1.85 %/sec). For the ripening of Ag NP regime, the slope of CF-3-HCHO+Au (-0.48 %/sec) is again comparable to the slope of CF-3-HCHO (-0.43 %/sec). The increased duration of the second regime for CF-3-HCHO+Au is due to an increased amount of activated Ag than the CF-3-HCHO sample. After second regimes, the successive Au(I) complex ions contact the Ag activated surface and initiated galvanic displacement of Ag by Au. The Ag and Au alloy formation results in a stable transmissivity for 60 sec.

However, the profile of BI-HCHO+Au, which is governed by unsteady state diffusion, exhibits a sharper drop and faster upshift of transmission relative to CF-3-HCHO+Au and CF-3-HCHO without a Ag NP ripening regime. The slope of Ag aggregation in BI-10m is -2.78 %/sec which is  $\sim 1.5$  times lower than CF-3-10, which is due to a faster mass transfer rate of HCHO induced by the near-instantaneous injection ( $\sim 1$  sec). For hydraulic condition of unsteady state diffusion for desired 10 min deposition, the 0.5 ml total mixture of Au solution and reducing agent was first injected into the flow cell for 1-sec and then incubated for 10 min. Due to rapid injection, the BI-EL mass transfer model needs to be modified to consider the instantaneous CF effect at the early stage of EL deposition. In CF-EL deposition, as flowrate increases, the continuous laminar or turbulent bulk flow decreases the stagnant boundary layer adjacent to the wall, resulting in an increased mass transfer rate. In principle, the instantaneous injection ( $F=0.5$  ml/sec) at the beginning of BI-EL deposition induces an initially thinner stagnant boundary layer relative to CF-3-HCHO+Au ( $F=8.3 \times 10^{-4}$  ml/sec). This thinner boundary layer of BI-HCHO+Au, results in faster initial diffusion of the HCHO and Au(I) complex ions than for the CF-3-

HCHO+Au condition. The mass transfer coefficient of Au(I) complex and HCHO for instantaneous injection are  $2.7 \times 10^{-3}$  cm/sec and  $5.3 \times 10^{-3}$  cm/sec, which are ~8.5 times faster than in CF-3-HCHO+Au deposition ( $3.2 \times 10^{-4}$  cm/sec and  $6.2 \times 10^{-4}$  cm/sec). The instantaneous injection of Au(I) thus resulted in a galvanic displacement of Ag by Au earlier than that observed in CF-3-HCHO+Au. The instantaneous injection may also displace some weakly bound Ag NPs and unbounded reduced Ag resting on the surface.



	Ag NP aggregation	Ag NP ripening	Photosensitive displacement	Galvanic replacement
HCHO/Ag (steady, 3ml/hr)	-1.24 ( $R^2=0.98$ ) [0-12s]	-0.48 ( $R^2=0.97$ ) [13-23s]	0.39 ( $R^2=0.97$ ) [24-50s]	--
HCHO+Au/Ag (steady, CF-3-10)	-1.85 ( $R^2=0.95$ ) [0-15s]	-0.43 ( $R^2=0.98$ ) [16-25s]	0.02 ( $R^2=0.52$ ) [26-80s]	
HCHO+Au/Ag (Unsteady, BI-10)	-2.78 ( $R^2=0.94$ ) [0-5s]	--	0.31 ( $R^2=0.96$ ) [6-20s]	-0.31 ( $R^2=0.99$ ) [21-80s]

**Figure S4.** Optical characterization of heterogeneous physicochemical reactions during initial EL Au deposition with varying diffusion conditions. The initial reaction may be categorized to Ag NP aggregation, Ag NP ripening, photosensitive displacement of Ag NP and galvanic replacement of Ag by Au.

## **6. Correlation of dynamic transmission profile between 50 sec and 300 sec with mass transfer model.**

Figure S5(A) exhibits the Au PL transmission drop in the specific range of 50-300 sec, the early time zone, also represent the specific amount of Au ion deposition. The correlation also suggests that the dynamic transmission drop in the range of 20–45 % represents the specific amount of Au ion deposited in the range of  $3.5\text{--}7.5\times 10^{-5}$  g/cm<sup>2</sup> for 250 sec deposition. Figure S5(B) shows that the negative slopes of Au PL profile between 50 and 300 sec corresponds to predicted mass transfer coefficients profile as a function of Reynolds number from 0.1 to 1.0. The correlation of negative slopes of Au PL profiles in the range of 0.08 – 0.18 %/s is well fitted for the profile of mass transfer coefficients in the range of  $2.0\text{--}3.0\times 10^{-4}$  cm/s. This suggests that the negative slope of Au PL profiles can be used to accurately represent mass transfer coefficients in CF-EL deposition. The abscissa error-bars are due to variations in flow cell dimension.

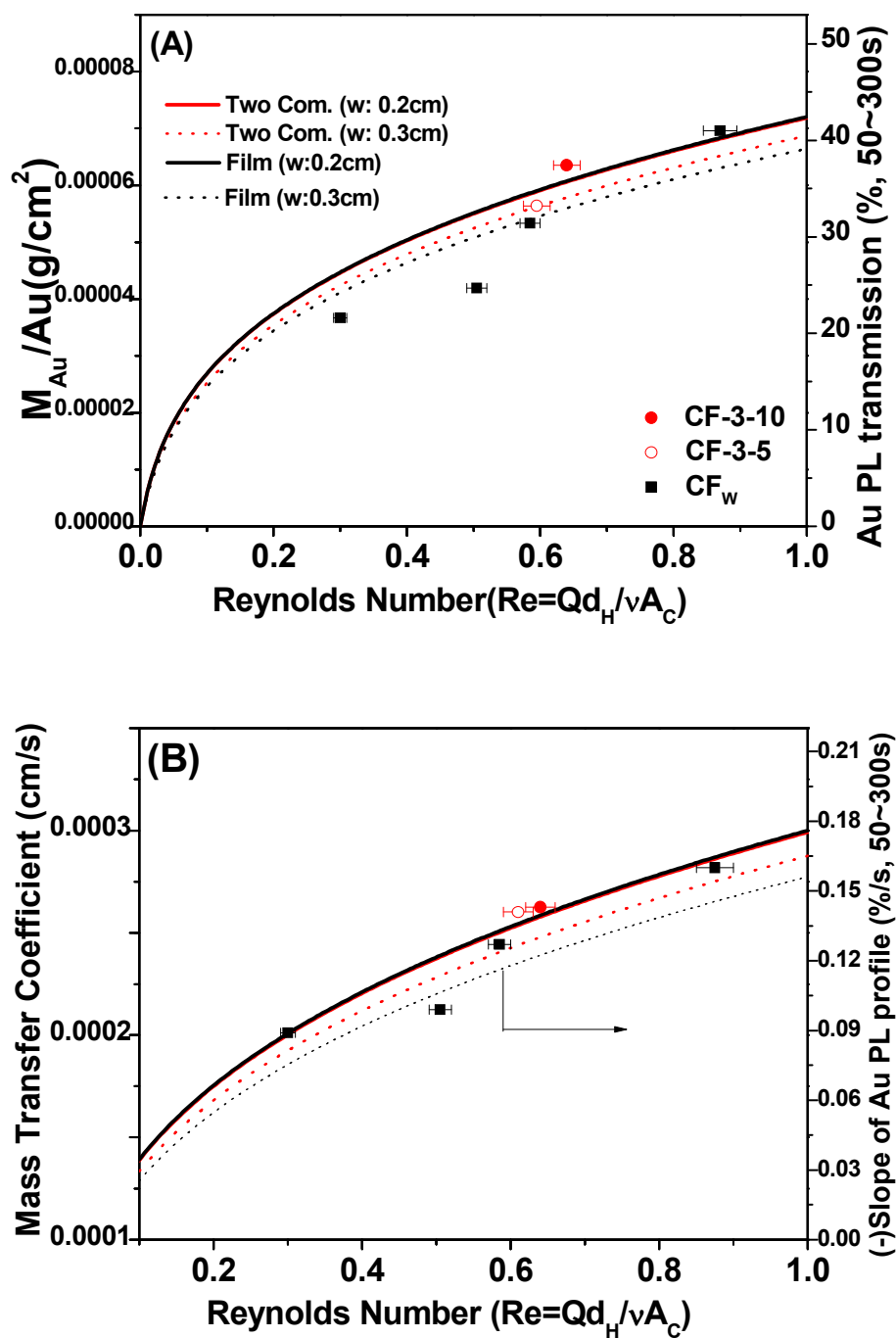


**Figure S5.** Correlations between coefficients of mass transfer model and dynamic optical features as a function of Reynolds number: (A) Correlation between specific deposition amounts and Au PL transmission drop values between 50 s and 300 s; (B) Correlation between mass transfer coefficients and slopes of Au PL profiles between 50 s and 300 s.

## 7. References

---

- (1) Singer, R. R.; Leitner, A.; Aussenegg, F. R., *J. Opt. Soc. Am. B*, **1995**, *12*, 220-228.
- (2) Baba, K.; Okuno, T.; Miyagi, M., *Appl. Phys. Lett.* **1993**, *62*(5), 437-439.
- (3) Jang, G.G.; Roper, D.K. *Anal. Chem.* **2011**, *83*, 1836-1842.
- (4) Jang, G.G.; Roper, D. K. *J. Phys. Chem. C* **2009**, *113*, 19228-19236.
- (5) Ahn, W.; Taylor, B.; Dall'Asén, A. G.; Roper, D. K. *Langmuir*, **2008**, *24*, 4174-4184.
- (6) Sancho-Parramon, J.; Janicki, V.; Loncaric, M.; Zorc, H.; Bubcek, P.; Bernstorff, S. *Appl. Phys. A* **2011**, *103*, 745-748.
- (7) Kaiser, N. *Appl. Opt.*, **2002**, *41*(16), 3053-3060.
- (8) Jang, G.G.; Hawkridge, M.; Roper, D. K. *J. Mater. Chem.*, **2012**, *22*, 21942-21953.
- (9) Park, H.H.; Zhang, X.; Choi, Y.J.; Kim, H.; Park, H.H.; Hill, R.H. *J. Cera. Soc. Japan*, **2010**, *118*(11) 1002-1005.